PNAS
www.pnas.org

Supplementary Information for

Epithelial Cell Chirality Revealed By Three-Dimensional Spontaneous Rotation

Amanda S. Chin, Kathryn E. Worley, Poulomi Ray, Gurleen Kaur, Jie Fan, and Leo Q. Wan

Rensselaer Polytechnic Institute, Troy, NY, 12180 USA

Leo Q. Wan
Email: wanq@rpi.edu

This PDF file includes:

Figs. S1 to S10
Tables S1 to S3
Captions for movies S1 to S21

Other supplementary materials for this manuscript include the following:

Movies S1 to S21

www.pnas.org/cgi/doi/10.1073/pnas.1805932115

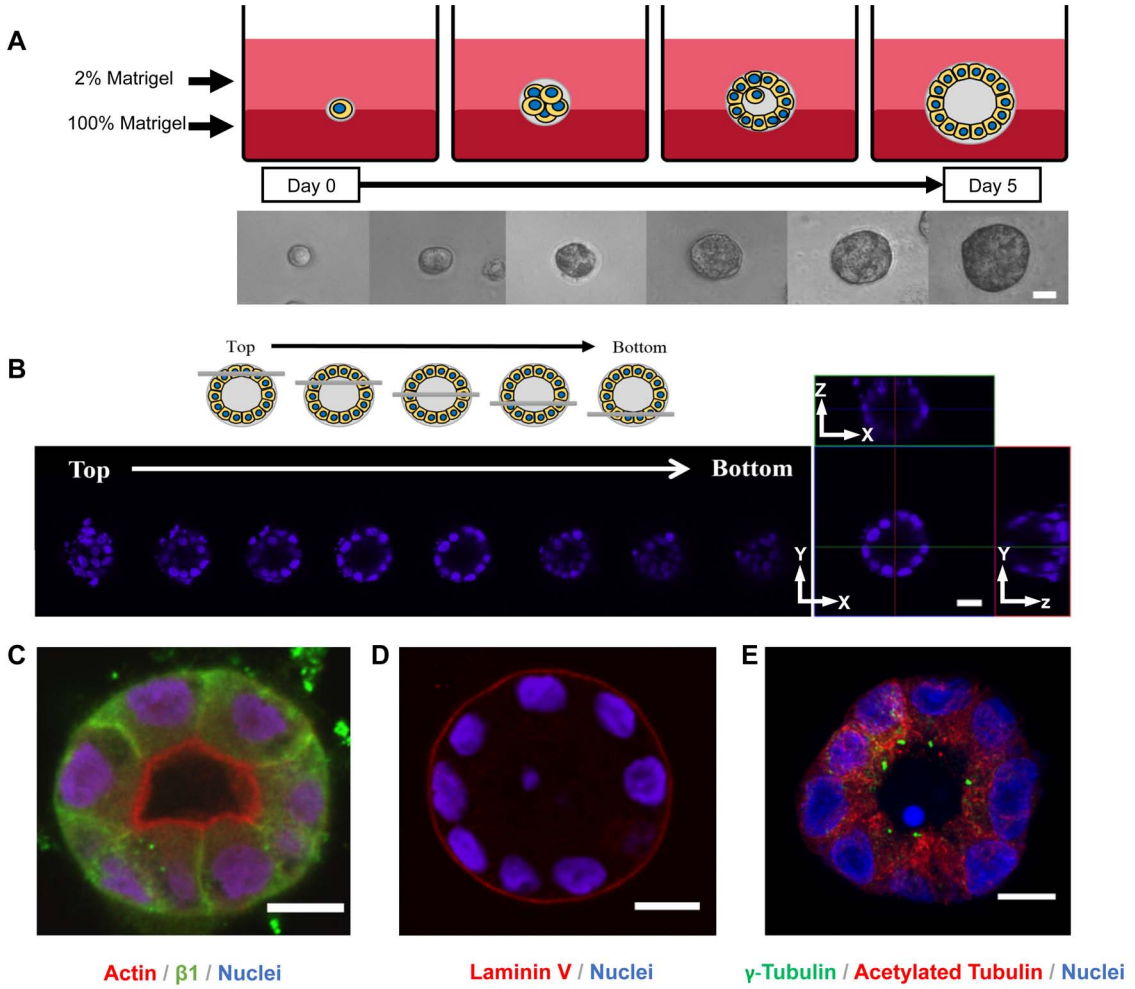

Fig. S1. MDCK cells self-organized and developed into luminal microspheroids in Matrigel. (**A**) Individual epithelial MDCK cells were embedded between a 100% Matrigel base layer and a 2% Matrigel top layer. The cells proliferated and formed microspheroids containing a lumen after 5 days of culture. Scale bar is 20 µm. (**B**) Confocal imaging of a MDCK microsphere at day 5 shown by z-stack images from top to bottom (left) and orthogonal projection (right). Scale bar is 20 µm. (**C-E**) Morphological architecture of the microspheroids was revealed using confocal microscopy to gather cross-sectional slice through the center of the microspheroids. The luminal spheroid structure exhibits a higher expression of actin along the apical surface (**C**) and significant basal accumulation of laminin (**D**), indicative of a polarized acinar formation. In addition, spheroids exhibit polarized cell organization with centrosomes (stained by γ-tubulin) positioning towards the apical surface, while no apparent cilia structures were noticed with acetylated tubulin staining (**E**). Scale bars are 10 µm.

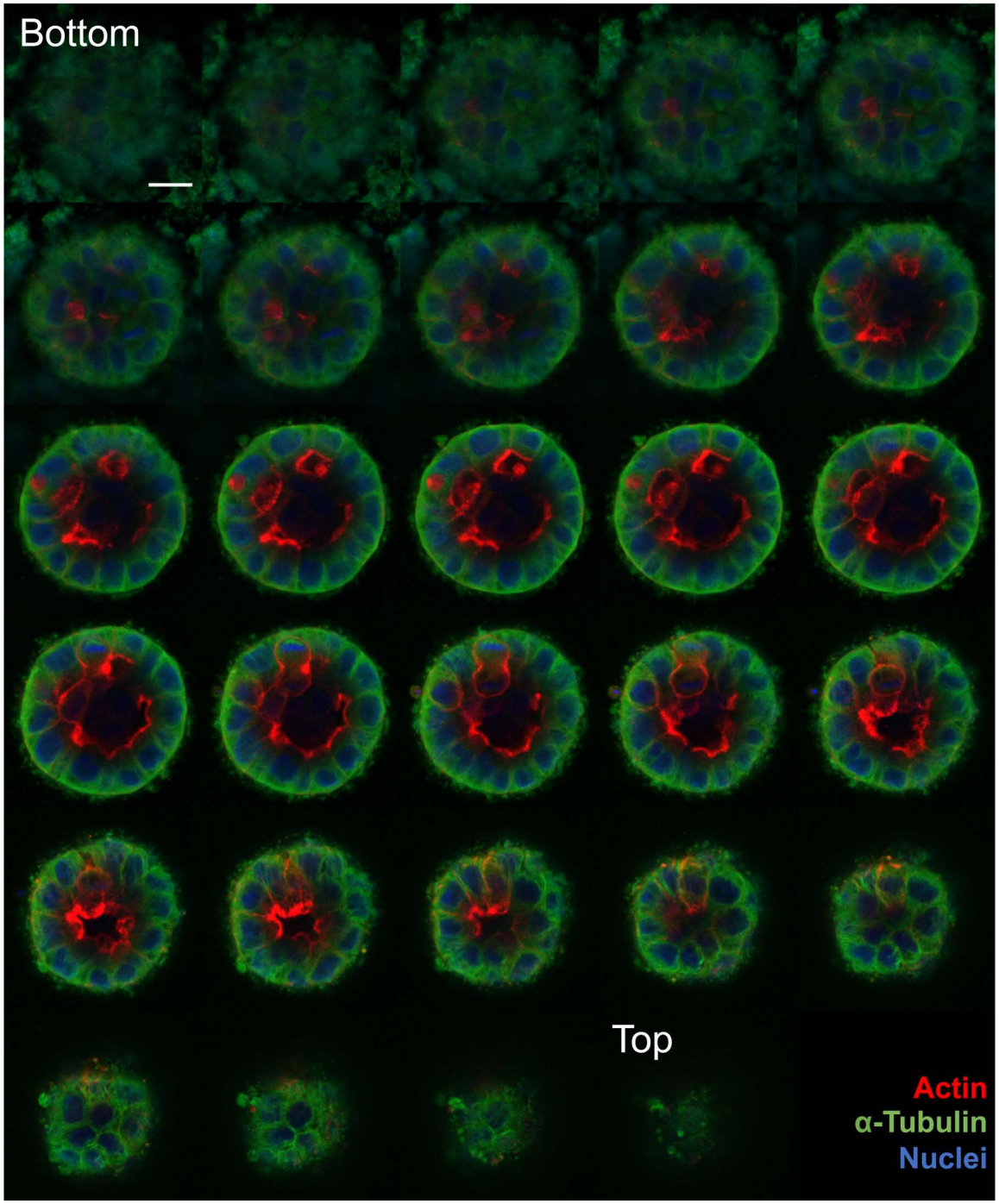

Fig. S2. Cytoskeletal structures of microspheroids in the 3D system. This montage depicts a z-stack of a day 5 microspheroid from bottom to top with each subsequent image (viewing each row from left to right) representing a step size of 1.7 μm in z-axis. Actin filaments (red) labeled with Phalloidin were localized along the cell boundaries with especially high expression along the apical surface. Microtubules labeled with an antibody for α-tubulin (green) exhibited radial alignment towards the basal surface in the microspheroid. Scale bar is 20 μm.

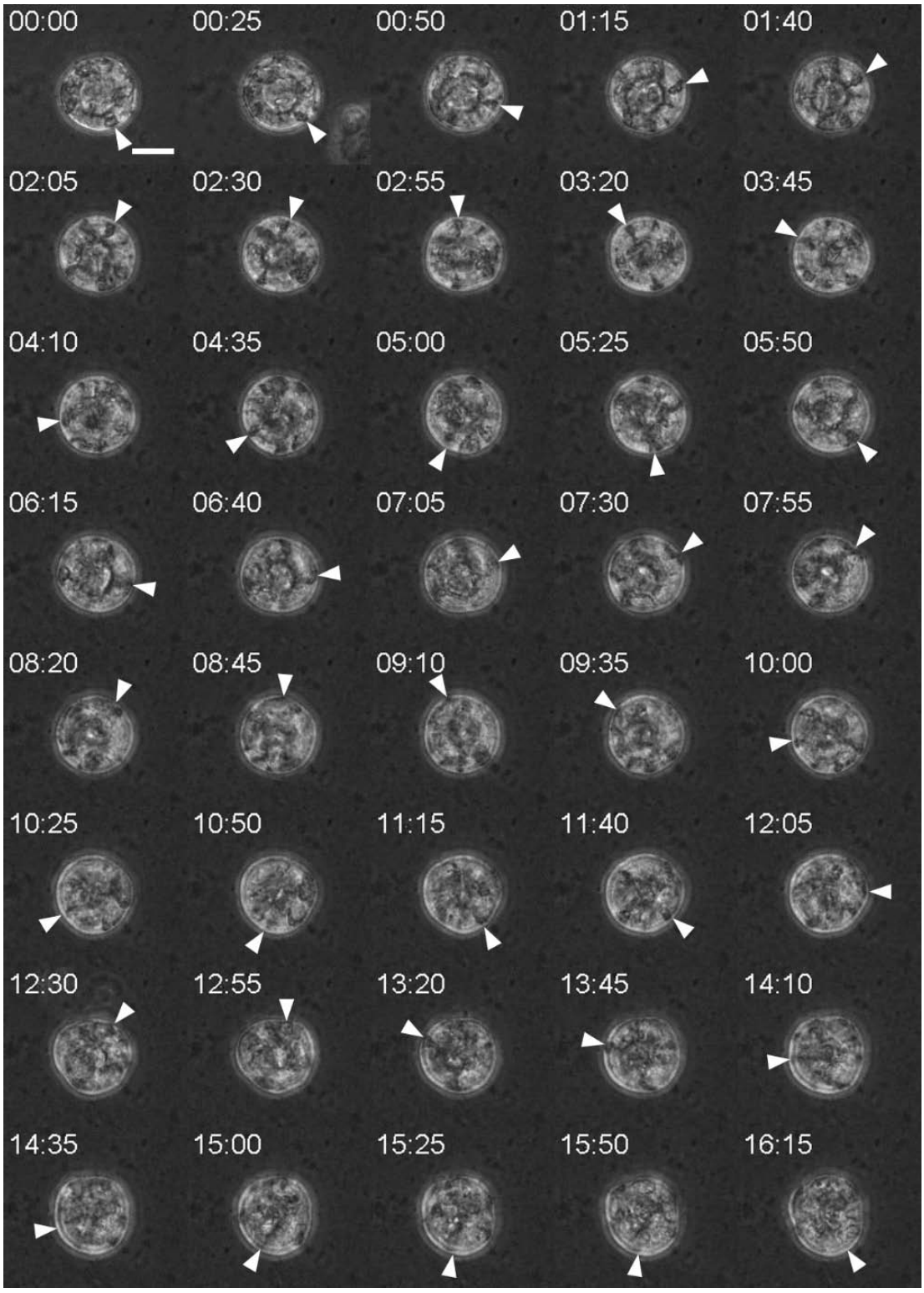

Fig. S3. A multicellular spheroid exhibits persistent chiral rotation for over 16 hours. This time-lapse montage displays the rotation of the spheroid at 25 minutes intervals with white arrows indicating a tracked position on the microsphere. Scale bar is 20 μm.

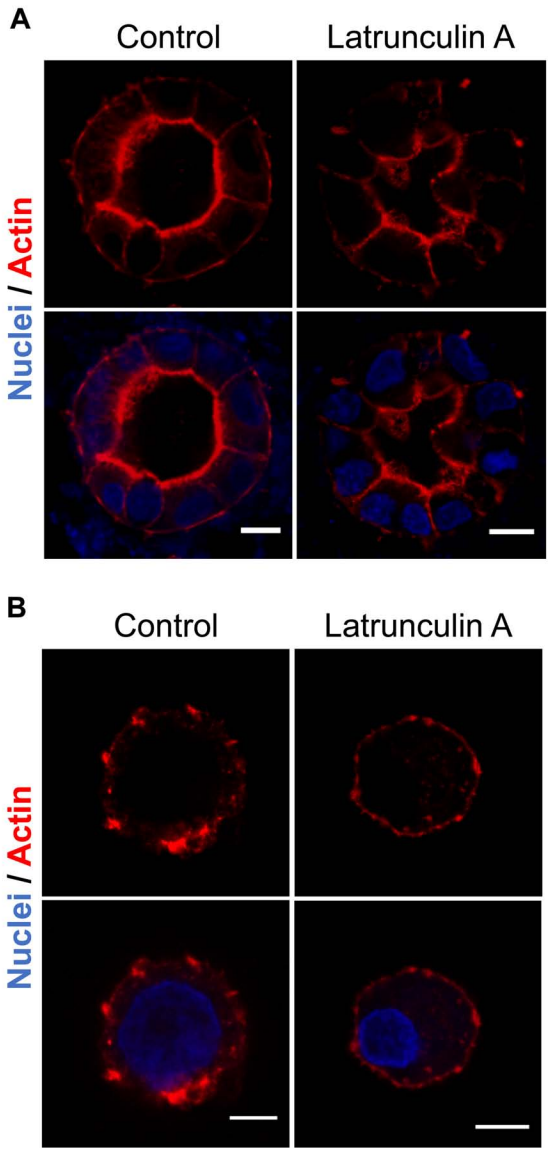

Fig. S4 Cell architecture and actin cytoskeleton structure are altered by Latrunculin A treatment. (**A**) Control microspheroids contain organized lumen with some basal actin and significant apical actin expression, while those treated with Latrunculin A for 4 hrs developed irregular lumen structures with less staining of actin. The scale bars are 10 μm. (**B**) Single cells exhibited clusters of strong actin localization along the cell boundary in the control group. In contrast, Latrunculin A treatments disperse the actin more evenly along the single cell boundary. The microspheroids and single cells were fixed and stained with Phalloidin for actin (red) and DAPI for nulcei (blue). The scale bars are 5 μm.

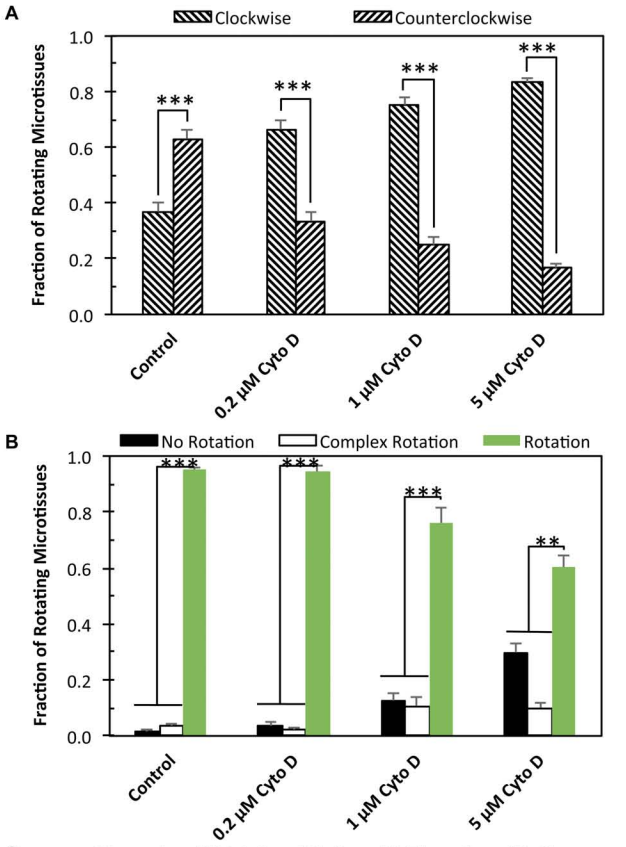

C

Microspheroid Rotational Motion with Disruption of Actin

Cytochalasin D Concentration	CW	CCW	No Rotation	Complex Rotation	p Value	Total
Control	72	**123**	3	7	0.00016	205
0.2 µM	**123**	62	7	4	4.3×10^{-06}	196
1 µM	**117**	39	26	22	1.5×10^{-10}	205
5 µM	**114**	23	68	23	5.45×10^{-16}	228

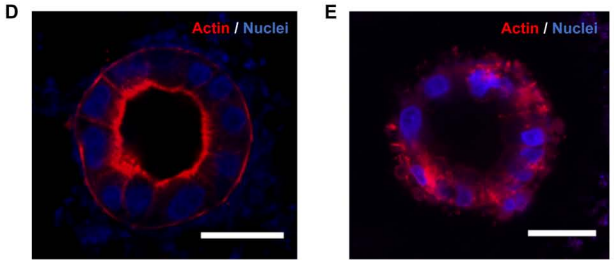

Fig. S5. 3D rotation bias is switched with inhibition of actin polymerization with cytochalasin D (Cyto D). (**A-C**) Chirality of 3D microspheriods was dominantly CCW in the untreated control and the biased direction of rotation was switched to be CW with 0.2 - 5 µM cytochalasin D treatment. Bold red numbers in (**C**) stand for a statistically bias toward the direction. **p < 0.01; ***p<0.001. (**D**) Untreated MDCK spheroids display apical actin localization with clear structure. (**E**) Cytochalasin D treatment for 4 hrs disrupted the assembly of the actin cytoskeleton in the spheroids resulting in fragmented structures. The spheroids were fixed and stained with Phalloidin for actin (red) and DAPI for nuclei (blue). Scale bars are 20 µm.

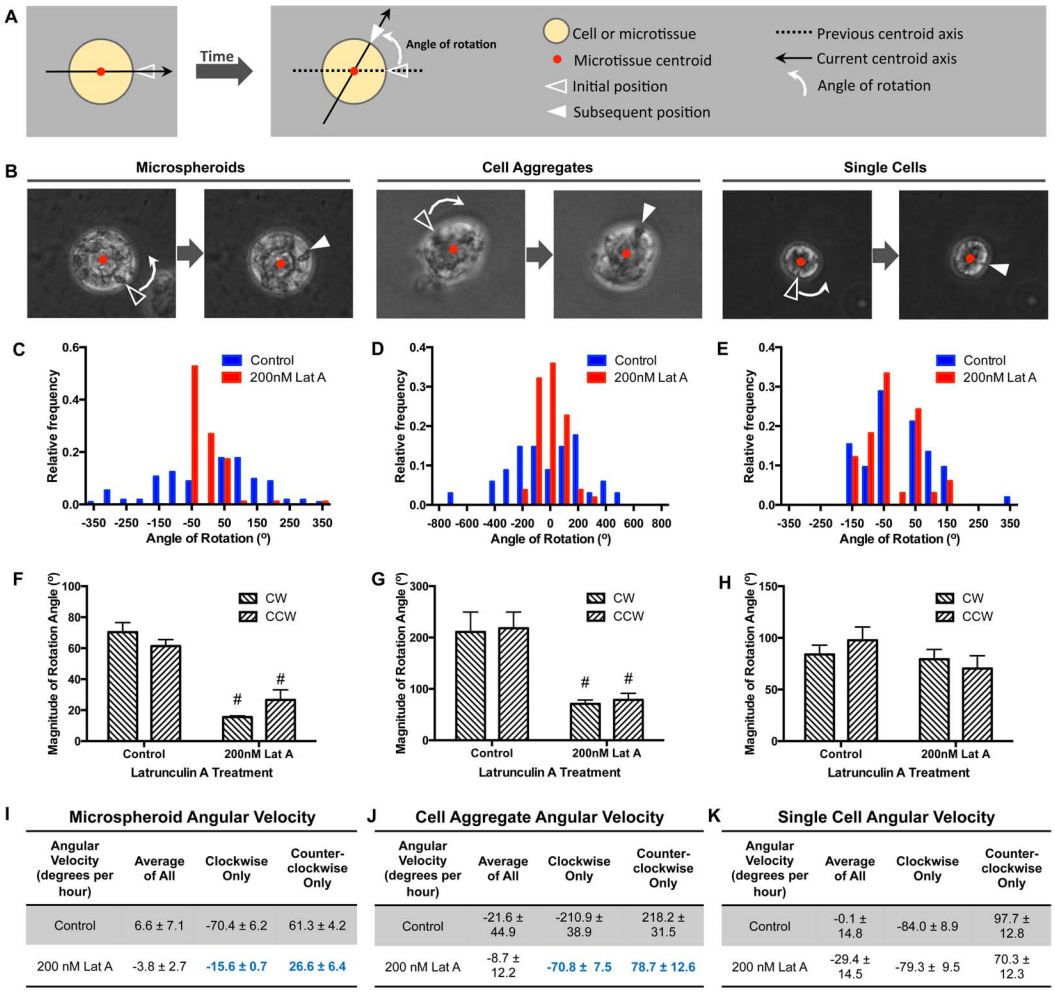

I Microspheroid Angular Velocity

Angular Velocity (degrees per hour)	Average of All	Clockwise Only	Counter-clockwise Only
Control	6.6 ± 7.1	-70.4 ± 6.2	61.3 ± 4.2
200 nM Lat A	-3.8 ± 2.7	**-15.6 ± 0.7**	**26.6 ± 6.4**

J Cell Aggregate Angular Velocity

Angular Velocity (degrees per hour)	Average of All	Clockwise Only	Counter-clockwise Only
Control	-21.6 ± 44.9	-210.9 ± 38.9	218.2 ± 31.5
200 nM Lat A	-8.7 ± 12.2	**-70.8 ± 7.5**	**78.7 ± 12.6**

K Single Cell Angular Velocity

Angular Velocity (degrees per hour)	Average of All	Clockwise Only	Counter-clockwise Only
Control	-0.1 ± 14.8	-84.0 ± 8.9	97.7 ± 12.8
200 nM Lat A	-29.4 ± 14.5	-79.3 ± 9.5	70.3 ± 12.3

Fig. S6. Characterization of rotational velocity of Latrunculin A treated microspheriods, aggregates and single cells within the 3D bilayer system. (**A**) Schematic illustrating how the rotation angle was measured in order to determine the angular velocity of microtissue rotation. The angle of rotation was measured between the initial centroid axis and the subsequent centroid axis. These axes are generated by the tracked microtissue position and the centroid of the microtissue. (**B**) Phase contrast time-lapse images of the microspheroid, cell aggregate and single cell with tracked positions indicated by white arrowheads. The angular velocity was quantified for (**C**, **F** & **I**) day 5 multicellular microspheriods, (**D**, **G** & **J**) cell aggregates, and (**E**, **H** & **K**) single cells. (**C-E**) are histograms of the distribution of rotation angles of microtissues for the control and 200 nM Latrunculin A treated groups, with the relative frequency representing the fraction of times a rotation angle occurred. (**F-H**) show the magnitude of rotation speed of microspheriods rotated in the CW and CW directions in degrees per hour. This magnitude was the absolute value of the angle of rotation. # indicates a significant difference in the Lat A treated group from the control. Tables (**I-K**) of average angular velocity of the rotating microtissues are shown on the bottom. The angular velocity is the rate at which a position on the microtissue rotates around the microtissue centroid. Positive angular velocity is indicative of CCW rotation and negative angular velocity represents CW. Bold blue numbers stand for a statistical difference between the Lat A treated group and the control group ($p<0.05$).

A

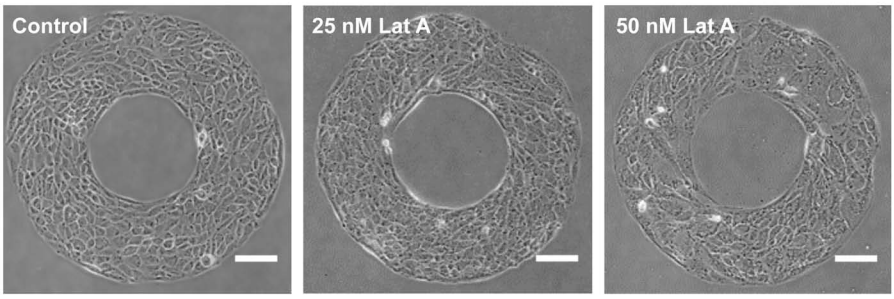

B

Chirality on Micropatterned Rings

2D Patterning	CW	NC	CCW	p Value	Total
Control	50	76	60	0.1955	186
25 nM Lat A	**18**	3	0	3.81×10^{-6}	21
50 nM Lat A	**65**	14	3	1.78×10^{-16}	82

Fig. S7. Chiral bias of MDCK on 2D micropatterned rings was reversed with actin inhibition via Latrunculin A treatment. MDCK on ring patterns exhibited slight bias towards CCW alignment. Latrunculin A treatment (25 -50 nM) of the MDCK cells on rings resulted in highly significant CW bias. (**A**) Phase contrast images of MDCK rings gathered at 10x magnification. Scale bars are 100 μm. (**B**) MDCK chirality on micropatterned surfaces under Latrunculin A treatment (25 nM and 50 nM). Bold red numbers stand for a statistical bias toward the specific direction. CW: clockwise alignment; CCW: counterclockwise alignment; NC: nonchiral or not significantly biased to CW or CCW.

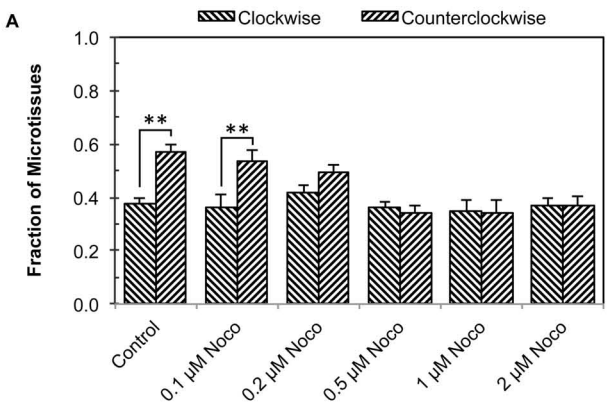

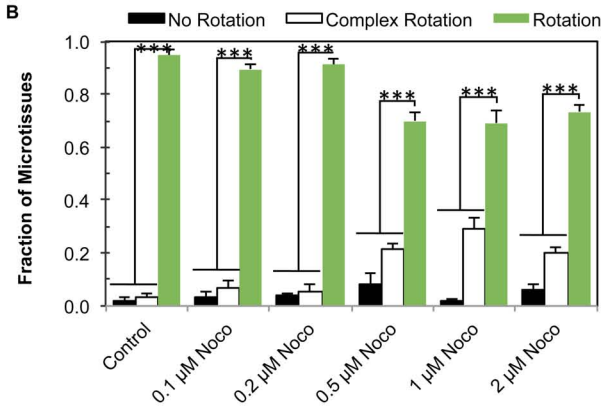

C

Microspheroid Rotational Motion with Disruption of Microtubules

Nocodazole Concentration	CW	CCW	No Rotation	Complex Rotation	p Value	Total
Control	59	**89**	3	5	0.0084	156
0.1 μM	83	**122**	8	16	0.0039	229
0.2 μM	102	121	9	13	0.1140	245
0.5 μM	47	44	11	28	0.4170	130
1 μM	61	60	3	51	0.5000	175
2 μM	65	65	11	36	0.5349	177

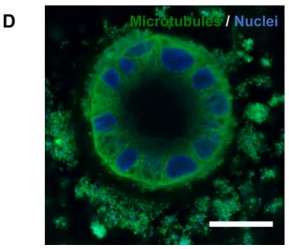

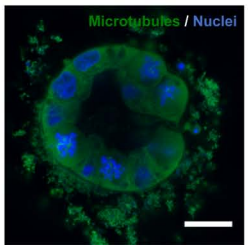

Fig. S8. 3D rotation bias of microspheroids is disrupted with Nocodazole (Noco) treatment. (**A-C**) Chirality of 3D microspheriods was dominantly CCW in the untreated control and the bias was lost with 0.2 - 5 μM Noco treatment. Bold red numbers in (**C**) stands for a statistically significant directional bias. **$p < 0.01$; ***$p<0.001$. (**D**) Microtubules exhibited radial alignment between the cells and strong presence at the basal surface in the control group. (**E**) Microspheroids treated with Noco for 4 hrs resulted in microtubule depolymerization. The spheroids were fixed and immunostained for α-tubulin for microtubules (green) and DAPI for nuclei (blue). Scale bars are 20 μm.

A

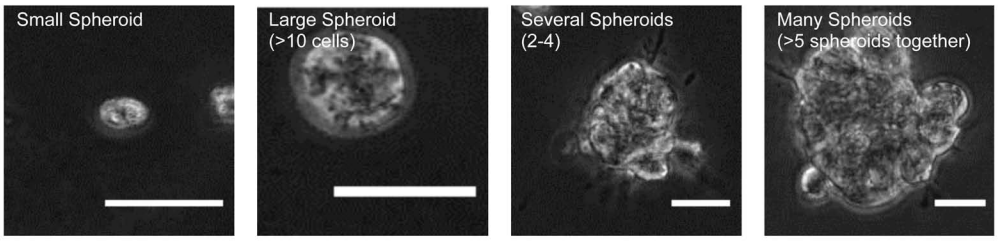

B

Chirality of Cell Aggregates by Size

Control Aggregates Data	CW	CCW	No Rotation	Rotation	Complex Rotation	p Value	Total
Small Spheroid	5	4	1	9	4	0.5000	14
Large spheroid (more than 10 cells)	12	11	4	23	16	0.5000	43
Several spheroids (2-4)	2	1	2	3	16	0.5000	21
Many Spheroids (>5 spheroids together)	0	0	0	0	10	-	10

C

Chirality of Large Spheroids Under Latruculin A treatment

Large Spheroid (>10 cells)	CW	CCW	No Rotation	Rotation	Complex Rotation	p Value	Total
Control	12	11	4	23	16	0.5000	43
100 nM Lat A	27	23	5	50	19	0.3359	74
150 nM Lat A	29	12	9	41	9	0.0058	59
200 nM Lat A	29	17	9	46	10	0.0519	65

Fig. S9. Rotational chirality of cell aggregates depends on aggregate size, organization, and actin. Aggregates ranged in size and were analyzed as four different categories: small spheroids (less than 10 cells), large spheroids (more than 10 cells), several spheroids (2-4 spheroids), and many spheroids (over 5 spheroids). (**A**) Representative phase contrast images of each type of cell aggregate category. Scale bars are 50 µm. (**B**) Rotational behavior of the aggregates was characterized for each type of aggregates. The three aggregate categories exhibited more complex rotational behavior in which the structures rotated out of plane and for larger aggregates, made of multiple spheroids, the spheroids would rotate in different directions. (**C**) Large spheroids (>10 cells) exhibited an increase in CW rotational behavior with Latrunculin A treatments.

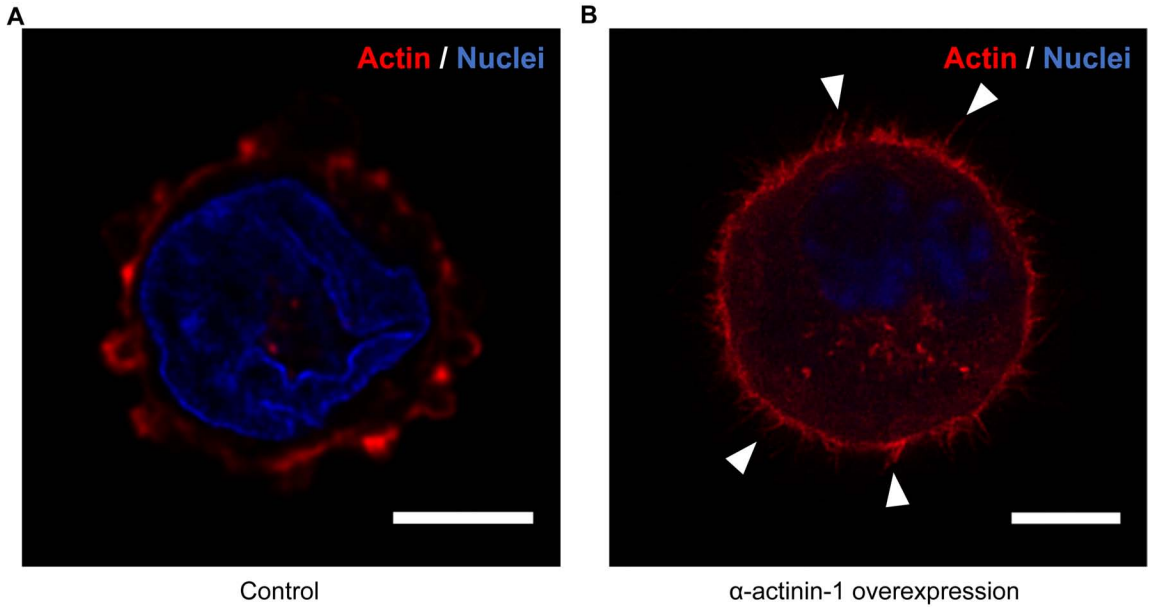

Fig. S10. Actin bundle structures develop along the cell borders of single cells with overexpression of α-actinin-1. Compared to the control cells (**A**), MDCK cells with α-actinin-1 overexpression (**B**) exhibited actin bundle structures that extend radially and often exhibit tilting, as indicated by white arrowheads. The single cells were fixed and stained with phalloidin for actin filaments (red) and DAPI for nuclei (blue). The scale bars are 5 μm.

Table S1. Chiral in-plane rotation is lost in the absence of biomaterial gradient. When MDCK cells were embedded between Matrigel bilayers of the same concentration (both 100%) the coherent rotation of microtissues became complex. The cells rotated through various planes and there was no clear bias in either CW or CCW direction**.**

Mechanical Gradient	Clockwise	Counter-clockwise	No Rotation	Rotation	Complex Rotation	p Value	Total
Single Stiffness - both layers 100% Matrigel	14	18	21	32	66	0.2983	119

Table S2. Chiral bias of two cell types observed in the 3D system. Human mammary epithelial cells (MCF 10A) undergo predominantly clockwise (CW) rotation, while the MDCK epithelial cells are mostly counterclockwise (CCW). Mouse cardiomyocytes (HL-1) had a CW biased rotation. Bold red numbers stand for a statistically significant bias toward the specific direction.

Cell Type	CW	CCW	No Rotation	Rotation	Complex Rotation	p Value	Total
MCF 10A	**72**	32	12	104	9	5.48×10^{-5}	125
HL-1	**62**	44	0	106	9	0.04912	115

Table S3. Chiral bias in direction of rotational behavior in the two-cell phase. The two-cell phase was observed 24 hrs after the MDCK cells were embedded within the bilayer. At this time point, the single cells have undergone division to form pairs of cells that exhibit obvious rotational behavior. Treatment with 50 nM Latrunculin (Lat) A caused a significant increase in CW rotation. Bold red numbers indicate a statistically significant bias toward the specific direction.

Bi-cell Rotation	CW	CCW	No Rotation	Rotation	Complex Rotation	p Value	Total
Control	107	**164**	8	279	36	5.97×10^{-5}	315
50 nM Lat A	**240**	132	18	379	32	1.82×10^{-4}	422

Movie S1. 3D reconstructed video of actin structures of the top half of a multicellular microspheroid after 5 days of culture. Actin was stained with Phalloidin.

Movie S2. 3D reconstructed video of actin structures of the bottom half of a multicellular microspheroid after 5 days of culture. Actin was stained with Phalloidin.

Movie S3. Phase contrast time-lapse of MDCK multicellular microspheroids (control) on the 5th day of culture. These day 5 microspheroids developed from single cells embedded within the bilayer Matrigel system. Red arrows indicate clockwise rotation. Cyan arrows indicate counterclockwise rotation. Black arrows indicate no rotation. White arrows indicate complex rotation through several planes. The frame rate is 50 fps, time interval between consecutive frames is 1 min, and the total duration of the time-lapse is 2 hrs.

Movie S4. Magnified time-lapse video of day 5 microspheroids. These day 5 microtissues developed from single cells embedded within the bilayer Matrigel system. The frame rate is 30 fps, the time interval between frames is 5 min, and the total time is 16.6 hrs.

Movie S5. Time-lapse video of MDCK multicellular microspheroids treated with Latrunculin A on the 5th day of culture. The frame rate is 50 fps, the time interval between each frame is 1 min, and the total duration of the time-lapse is 2 hrs.

Movie S6. Magnified time-lapse video of day 5 microspheroids treated with Latrunculin A. The frame rate is 30 fps, the time interval between frames is 5 min, and the total time is 24 hrs.

Movie S7. 3D reconstructed video of actin structures of the top half of a day 5 multicellular microspheroid, treated with 200nM Latrunculin A for 4 hrs. Actin was stained with Phalloidin.

Movie S8. 3D reconstructed video of actin structures of the bottom half of a day 5 multicellular microspheroid, treated with 200nM Latrunculin A for 4 hrs. Actin was stained with Phalloidin.

Movie S9. Phase contrast time-lapse video of a small spheroid (less than 10 cells) cell aggregate. Aggregates ranged in size and were analyzed as four different categories: small spheroids (less than 10 cells), large spheroids (more than 10 cells), several spheroids (2-4 spheroids), and many spheroids (over 5 spheroids). The frame rate is 50 fps, the time interval between frames is 1 min, and the total time is 2 hrs.

Movie S10. Phase contrast time-lapse video of a large spheroid (more than 10 cells) cell aggregate. Aggregates ranged in size and were analyzed as four different categories: small spheroids (less than 10 cells), large spheroids (more than 10 cells), several spheroids (2-4 spheroids), and many spheroids (over 5 spheroids). The frame rate is 50 fps, the time interval between frames is 1 min, and the total time is 2 hrs.

Movie S11. Phase contrast time-lapse video of a cell aggregate made of several (2-4) spheroids. Aggregates ranged in size and were analyzed as four different categories: small spheroids (less than 10 cells), large spheroids (more than 10 cells), several spheroids (2-4 spheroids), and many spheroids (over 5 spheroids). The frame rate is 50 fps, the time interval between frames is 1 min, and the total time is 2 hrs.

Movie S12. Phase contrast time-lapse video of a cell aggregate made of many spheroids (over 5 spheroids). Aggregates ranged in size and were analyzed as four different categories: small spheroids (less than 10 cells), large spheroids (more than 10 cells), several spheroids (2-4 spheroids), and many spheroids (over 5 spheroids). The frame rate is 50 fps, the time interval between frames is 1 min, and the total time is 2 hrs.

Movie S13. Phase contrast time-lapse video of cell aggregates under Latrunculin A treatment. This large spheroid (containing more than 10 cells) was treated with 100 nM Latrunculin A. The frame rate is 50 fps, the time interval between frames is 1 min, and the total time is 2 hrs.

Movie S14. 3D reconstructed video of actin structures of the top half of a single MDCK cells. Actin was stained with Phalloidin, and nuclei were stained with DAPI (blue).

Movie S15. 3D reconstructed video of actin structures of the bottom half of a single MDCK cells. Actin was stained with Phalloidin, and nuclei were stained with DAPI (blue).

Movie S16. Overlaid live fluorescence time-lapse video of single cells (blue: nuclei and red: Golgi apparatuses). Single cells were embedded within the bilayer Matrigel system and time-lapse for single cells gathered 2 hrs after seeding. The track is shown in green. The frame rate is 10 fps, the interval between frames is 5 min, and the duration of the time-lapse is 4 hrs.

Movie S17. Overlaid live fluorescence time-lapse video of Latrunculin A-treated single cells (blue: nuclei and red: Golgi apparatuses)**.** Single cells embedded within the bilayer Matrigel system and time-lapse for single cells were gathered 2 hrs after seeding. The track is shown in green. The frame rate is 10 fps, the interval between frames is 5 min, and the duration of the time-lapse is 4 hrs.

Movie S18. Phase contrast time-lapse of two-cell bodies. These time-lapse were gathered 24 hrs after single cells were embedded within the bilayer Matrigel system. The single cells were able to divide and form pairs of cells, which rotated very fast in the bilayer system. Red arrows indicate clockwise rotation. Cyan arrows indicate counterclockwise rotation. Black arrows indicate no rotation. White arrows indicate complex rotation through several planes. The frame rate is 20 fps, time interval between each frame is 5 min, and the total duration of the time-lapse is ~6 hrs.

Movie S19. Phase contrast time-lapse of two-cell bodies treated with 50 nM Latrunculin A. These time-lapse were gathered 24 hrs after single cells were embedded within the bilayer Matrigel system. The single cells were able to divide and form pairs of cells, which rotated very fast in the bilayer system. Red arrows indicate clockwise rotation. Cyan arrows indicate counterclockwise rotation. Black arrows indicate no rotation. White arrows indicate complex rotation through several planes. The frame rate is 20 fps, time interval between each frame is 5 min, and the total duration of the time-lapse is 4.5 hrs.

Movie S20. 3D reconstructed video of actin structures of the top half of a single MDCK cells with α-actinin-1 overexpressed. Actin was stained with Phalloidin, and nuclei were stained with DAPI (blue).

Movie S21. 3D reconstructed video of actin structures of the bottom half of a single MDCK cells with α-actinin-1 overexpressed. Actin was stained with Phalloidin, and nuclei were stained with DAPI (blue).